stabilized by polyvalent polymer–colloid interactions. Roughly spherical aggregates of similar dimensions (~60 nm) were obtained from 6-nm analogues of Thy-Au and polymer **1** (see Supplementary Information), demonstrating the applicability of our polymer-mediated approach to the assembly of different sized nanoparticle subunits.

Self-assembly processes are governed by a balance of entropic and enthalpic effects, making them very temperature dependent. This temperature dependence is manifested by more efficient recognition processes at lower temperatures[21], which would be expected to yield larger aggregate structures. Investigations of temperature effects on the preparation of the aggregates yielded results consistent with this prediction. TEM micrographs of the precipitate formed at −20 °C revealed the formation of microscale (0.5–1 μm) discrete spherical particles (Fig. 5b), consisting of $(6–50) \times 10^5$ individual Thy-Au units. These microscale particles are among the most complex synthetic self-assembled structures known, demonstrating the thermal control of aggregate size using the 'bricks and mortar' methodology.

In addition to controlling the size of the aggregates, temperature strongly affects the morphology of the resulting ensembles. At 10 °C, networks were formed (Fig. 5c), as opposed to the discrete structures observed at higher and lower temperatures. This suggests that network formation is an intermediate process in the formation of the giant assemblies at −20 °C. The individual assemblies within these networks remained spherical, although their sizes are more highly dispersed. We are currently investigating methods aimed at achieving control over the size and the geometry of these networks, which would allow the fabrication of rod- and wire-like structures for incorporation in nanoscale constructs (see Supplementary Information).

We have demonstrated a polymer-mediated strategy for the self-assembly of nanoparticles into structured ensembles. Discrete microspheres formed using this methodology are truly multi-scale constructs, highly ordered on the molecular, nanometre and micrometre scale. This method has also been shown to generate network structures, which can serve as precursors to other shapes and sizes of nanoparticle assembly. The degree of ordering and the control of particle size and shape, coupled with the inherent modularity of the 'bricks and mortar' colloid-polymer self-assembly process, represent a powerful and general strategy for the creation of highly structured multifunctional materials and devices. □

Received 8 July 1999; accepted 10 February 2000.

1. Anelli, P. L., Spencer, N. & Stoddart, J. F. A molecular shuttle. *J. Am. Chem. Soc.* **113,** 5131–5133 (1991).
2. Otsuki, J. *et al.* Redox-responsive molecular switch for intramolecular energy transfer. *J. Am. Chem. Soc.* **119,** 7895–7896 (1997).
3. de Silva, A. P., Gunaratne, H. Q. N. & McCoy, C. P. Molecular photoionic and logic gates with bright fluorescence and "off-on" digital action. *J. Am. Chem. Soc.* **119,** 7891–7892 (1997).
4. Alivisatos, A. P. From molecules to materials: Current trends and future directions. *Adv. Mater.* **10,** 1297–1336 (1998).
5. Breen,T. L., Tien, J., Oliver, S. R. J., Hadzic, T. & Whitesides, G. M. Design and self-assembly of open, regular, 3D mesostructures. *Science* **284,** 948–951 (1999).
6. Lehn, J.-M. *Supramolecular Chemistry* (VCH, Weinheim, 1995).
7. Fyfe, M. C. T. & Stoddart, J. F. Synthetic supramolecular chemistry. *Acc. Chem. Res.* **30,** 393–401 (1997).
8. Rebek, J. Reversible encapsulation and its consequences in solution. *Acc. Chem. Res.* **32,** 278–286 (1999).
9. Stupp, S. I. *et al.* Supramolecular materials: Self-organized nanostructures. *Science* **276,** 384–389 (1997).
10. Kotera, M., Lehn, J. -M. & Vigneron, J. -P. Self-assembled supramolecular rigid rods. *J. Chem. Soc. Chem. Commun.* 197–199 (1994).
11. Edgecombe, B. D., Stein, J. A., Fréchet, J. M. J., Xu, Z. & Kramer, E. J. The role of polymer architecture in strengthening polymer-polymer interfaces: A comparison of graft, block, and random copolymers containing hydrogen-bonding moieties. *Macromolecules* **31,** 1292–1304 (1998).
12. Andres, R. P. *et al.* Self-assembly of a two-dimensional superlattice of molecularly linked metal clusters. *Science* **273,** 1690–1693 (1996).
13. Markovich, G. *et al.* Architectonic quantum dot solids. *Acc. Chem. Res.* **32,** 415–423 (1999).
14. Liu, J. *et al.* Cyclodextrin-modified gold nanospheres. Host-guest interactions at work to control colloidal properties. *J. Am. Chem. Soc.* **121,** 4304–4305 (1999).
15. Marinakos, S. M., Brousseau, L. C. III, Jones, A. & Feldheim, D. L. Template synthesis of one-dimensional Au, Au-poly(pyrrole), and poly(pyrrole) nanoparticle arrays. *Chem. Mater.* **10,** 1214–1219 (1998).
16. Whetten, R. L. *et al.* Crystal structures of molecular gold nanocrystal arrays. *Acc. Chem. Res.* **32,** 397–406 (1999).
17. Mucic, R. C., Storhoff, J. J., Mirkin, C. A. & Letsinger, R. L. DNA-directed synthesis of binary nanoparticle network materials. *J. Am. Chem. Soc.* **120,** 12674–12675 (1998).
18. Mirkin, C. A., Letsinger, R. L., Mucic, R. C. & Storhoff, J. J. A DNA-based method for rationally assembling nanoparticles into macroscopic materials. *Nature* **382,** 607–609 (1996).
19. Alivisatos, A. P. *et al.* Organization of 'nanocrystal molecules' using DNA. *Nature* **382,** 609–611 (1996).
20. Boal, A. K. & Rotello, V. M. Redox-modulated recognition of flavin by functionalized gold nanoparticles. *J. Am. Chem. Soc.* **121,** 4914–4915 (1999).
21. Deans, R., Ilhan, F. & Rotello, V. M. Recognition mediated unfolding of a self-assembled polymeric globule. *Macromolecules* **32,** 4956–4960 (1999).
22. Park, T. K., Schroeder, J. & Rebek, J. New molecular complements to imides. Complexation to thymine derivatives. *J. Am. Chem. Soc.* **113,** 5125–5127 (1991).
23. Muehldorf, A. V., Van Engen, D., Warner, J. C. & Hamilton, A. D. Aromatic aromatic interactions in molecular recognition: a family of artificial receptors for thymine that shows both face-to-face and edge-to-face interactions. *J. Am. Chem. Soc.* **110,** 6561–6562 (1988).
24. Brust, M., Walker, M., Bethell, D., Schiffrin, D. J. & Whyman, R. Synthesis of thiol-derivatized gold nanoparticles in a 2-phase liquid-liquid system. *J. Chem. Soc. Chem. Commun.* 801–802 (1994).
25. Ingram, R. S., Hostetler, M. J. & Murray, R. W. Poly-hetero-omega-functionalized alkanethiolate-stabilized gold cluster compounds. *J. Am. Chem. Soc.* **119,** 9175–9178 (1997).

Supplementary information is available on *Nature*'s World-Wide Web site (http://www.nature.com) and as paper copy from the London editorial office of *Nature*.

Acknowledgements

This work was supported by the NSF. V.M.R. also acknowledges support from the Petroleum Research Fund of the ACS, the Center for University Research in Polymers at the University of Massachusetts, the Alfred P. Sloan Foundation, Research Corporation, and the Camille and Henry Dreyfus Foundation.

Correspondence and requests for materials should be addressed to V.M.R. (e-mail: rotello@chem.umass.edu).

Subduction erosion along the Middle America convergent margin

C. R. Ranero & R. von Huene

GEOMAR, Wischhofstrasse 1-3, Kiel 24148, Germany

'Subduction erosion' has been invoked to explain material missing from some continents along convergent margins[1]. It has been suggested that this form of tectonic erosion removes continental material at the front of the margin or along the underside of the upper (continental) plate[2–4]. Frontal erosion is interpreted from disrupted topography at the base of a slope and is most evident in the wake of subducting seamounts[5,6]. In contrast, structures resulting from erosion at the base of a continental plate are seldom recognized in seismic reflection images because such images typically have poor resolution at distances greater than ~ 5 km from the trench axis. Basal erosion from seamounts and ridges has been inferred[7,8], but few large subducted bodies—let alone the eroded base of the upper plate—are imaged convincingly. From seismic images we identify here two mechanisms of basal erosion: erosion by seamount tunnelling and removal of large rock lenses of a distending upper plate. Seismic cross-sections from Costa Rica to Nicaragua indicate that erosion may extend along much of the Middle America convergent margin.

From Costa Rica to Nicaragua the Pacific continental margin is formed by a wedge-shaped body of igneous rock (margin wedge), covered by 1–2 km of slope sediment and fronted by a small sediment prism[9–11]. The facing ocean plate has a variable structure; there is thick crust at the Cocos ridge[12], the plate is ~40% covered by seamounts off central Costa Rica, and has a smooth morphology off the northwest Nicoya peninsula (Fig. 1). Off Nicaragua, the subducting ocean crust is thin (~5 km) and cut by many normal faults with ~0.5-km displacement[11,13,14]. Variations of crustal structure and seafloor morphology of the subducting plate correspond with regional and local changes in upper-plate thickness along the margin. On a regional scale, the ocean crust thins and deepens towards Nicaragua, whereas the corresponding continental margin wedge thickens (Fig. 2). Where the buoyant Cocos ridge subducts, the margin wedge is thinner than opposite the adjacent seamount segment (Fig. 2). Facing the seamount segment the margin is thinner than to the northwest and is thinnest at a large embayment off the southeast Nicoya peninsula (Figs 1 and 2). The margin wedge thickens off the northwest Nicoya peninsula where the featureless sea floor subducts, and is even thicker off Nicaragua, where deep sea floor and thin crust subduct.

The thin margin wedge (Fig. 2) and indented continental slope (Fig. 1) opposite the seamounts and the Cocos ridge suggest that repeated seamount subduction is an effective agent of upper-plate erosion. Opposite the seamount segment the slope has several grooves parallel to the convergence vector (G1 to G4, Fig. 1). The grooves mark the path of subducting seamounts, and the local uplift at the end of G1, G2 and G4 indicates that three seamounts are underthrusted beneath the slope[14]. The grooves indicate missing upper-plate material associated with seamount subduction. Two upper-plate areas are eroded during seamount subduction. Seamount impact erodes the margin front producing re-entrant structures at the base of the continental slope (for example, G1 and G4, Figs 1 and 3a). Landward, in the 30–40 km of the margin upslope of the frontal prism, the margin wedge remains semi-coherent as seamount underthrusting uplifts, fractures and thins the upper plate. The resulting rough margin-wedge upper surface has relief locally exceeding 0.5 km (Fig. 3a, b). Discontinuous strata are locally folded parallel to the surface (Fig. 3b), and undeformed younger strata smoothes this topography. The rough surface and a disrupted canyon system are roughly coincident. Seismic images from areas where seamounts have subducted (for example, Fig 3a) and along the grooves of subducting seamounts[14] indicate that only the upper part of the slope sediment slides at the oversteepened slope above subducting seamounts. Although some of the slumped sediment is missing, it is not enough to explain the grooves. The groove G3 penetrates the most into the margin (Fig. 1) where it is a deep trough collecting sediment delivered by shallow canyons (Fig. 3a). Although the groove is partially filled with recent sediment, the anomalous depth indicates missing material and erosion at the base of the upper plate.

Where seamounts no longer disrupt the front of the margin wedge but tunnel beneath it, we have imaged active basal erosion. Above a seamount about 2 km high, 0.5–0.7 km of rock from the base of a 2-km-thick margin wedge is missing (Fig. 4), which helps to explain the grooves and the thin margin wedge at the embayments. It has been proposed that uplift of the decollement over a

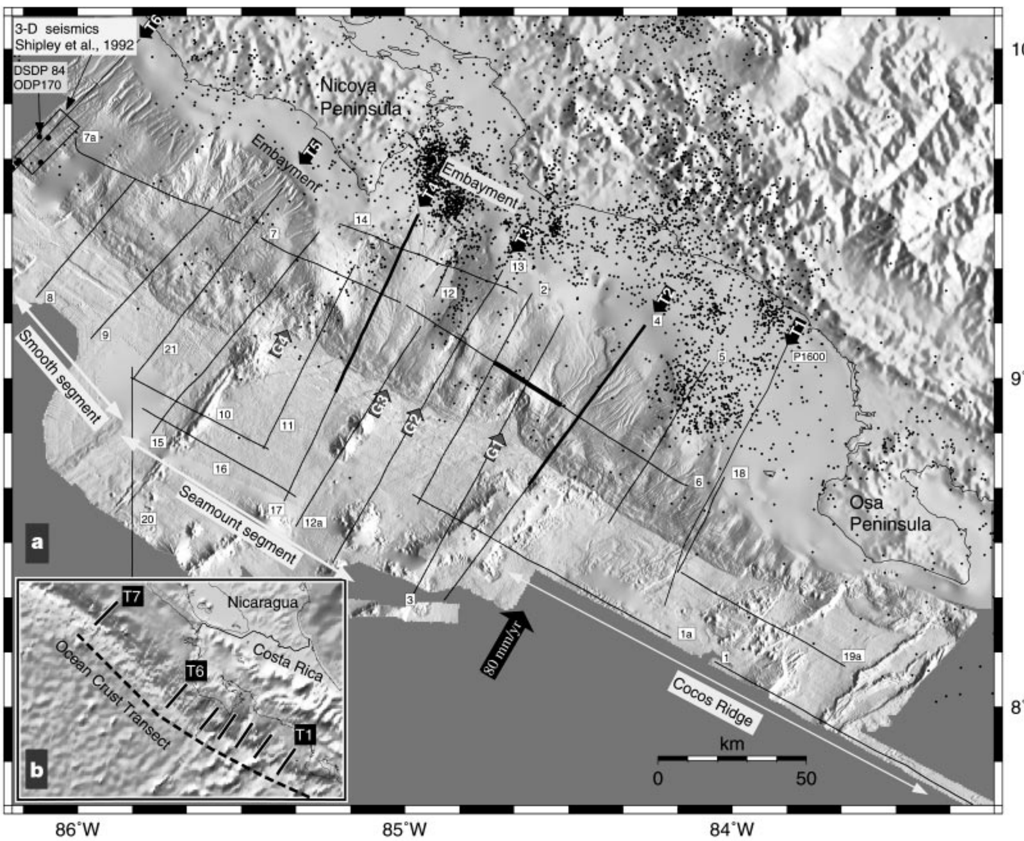

Figure 1 Bathymetry and tracks of seismic data off Costa Rica and Nicaragua. **a**, Multibeam hydrosweep bathymetry off Costa Rica with tracks of Sonne-81 and Shell P1600 multichannel seismic reflection data. The sudden change in roughness from the continental slope to the platform occurs where the multibeam bathymetry coverage ends. Bathymetry in the platform is from low-resolution maps. Thick lines mark segments shown in Figs 3 (lines 4 and 17) and 4, (line 6). Filled dots are earthquake epicentres[17]. Only earthquakes deeper than 30 km are plotted beneath the mainland. The ocean plate has three segments: the Cocos ridge with crust >12 km thick[12], the seamount segment with topographic features 1–2.5 km tall and 10–20 km wide, and a smooth seafloor segment off the northwest Nicoya peninsula. Subduction of seamounts is indicated by grooves in the continental slope (G1–G4) and clusters of earthquakes beneath the continental slope and shelf. Large embayments in the margin morphology indicate areas where seamount subduction has eroded the upper plate[14]. **b**, Location of the transect along the ocean plate (dashed line) and of the cross-sections T1–T7 used in Fig. 2. Cross-section T2 is a prestack depth migration. The other cross-sections are constrained by wide-angle and coincident near-vertical seismic data. Box off northwest Nicoya peninsula marks the area of a 3D seismic data set[19].

seamount might create a fluid pressure gradient that drains fluid from the seamount flanks and concentrates it at the crest, thereby promoting hydrofracturing and low friction[8]. However, the pervasive fracturing observed in the bathymetry at the crest of domes above subducting seamounts (Fig. 3a) provides fluids conduits for venting that probably relieve pressure. The increase in normal stress across the plate interface resulting from the accommodation of the seamount[15] in addition to the roughness of the volcano probably facilitates abrasion along the seamount subduction path[16]. Earthquakes of magnitude greater than 4 at the front of the margin[17] are located near the subducting seamounts and have strike-slip rather than thrust focal mechanisms, indicating a relatively high friction between seamounts and upper plate. Where the upper plate is >6–8 km thick, seamounts uplift but do not break up the margin wedge (Fig. 3a), so its upper surface is smooth, disrupted only by landward dipping normal faults that extend into the overlying strata (Fig. 3c).

On several seismic lines, plate-boundary reflections deeper than ~ 6 km bifurcate and surround megalenses (10–15 km long, 1.5–2 km high) whose origin is puzzling (Fig. 3a and d). Similar structures are observed off the northwest Nicoya peninsula[18,19]. The megalenses occur in areas where the upper plate extends by normal faulting, and could represent material transferred from the lower to the upper plate (for example, underplated sediment or a sheared-off seamount) or alternatively margin-wedge rock transferred to the lower plate. The size in two dimensions of some megalenses is equivalent to a seamount (Fig. 3d), so if they had been transferred from lower to upper plate the uplift should resemble that of currently underthrusting seamounts. However, seismics and bathymetry (Fig. 3d) show no large doming, but rather a relatively stable slope with a canyon system, and also a less disrupted margin wedge and slope sediment than along seamount paths, inconsistent with a subducting or sheared-off seamount. Underplating might require more time and thus the slope may have stabilized, but the ~ 2-km-thick lens would require a large uplift of the margin wedge (see, for example, Fig. 4) which is not observed (Fig. 3d). Thus, the megalenses are probably being removed from the upper plate. Further support for erosion comes from the style of normal faulting. Some reflections from the landward-dipping fabric of events within the margin wedge project to offsets at the top, indicating that normal faults cut deep into the upper plate. Landward-dipping, deep-penetrating normal faulting has also been described in the middle slope off northwest Nicoya[18]. On line 4, fault dip decreases and fault throw grows trenchwards (Fig. 3e), with the largest fault throws seaward of the megalens where the margin wedge is thinner (Fig. 3d). Extension, thinning and collapse of the margin seaward of the megalens is the response to the material transfer. The megalenses occur at depths at which temperatures calculated from depth to bottom-simulating reflectors indicate that the smectite–illite transition has occurred, and the plate interface is entering the zone of stick-slip behaviour[20]. Thus, the lenses could be associated with active erosion in an environment of increasing friction. This mechanism has no apparent relation to seamount subduction, and might be active in other areas where relatively smooth ocean floor is subducted. Beneath the upper slope, the upper boundary of the megalenses is a linear splay from the plate-boundary interface at about 10–11 km depth. The landward-dipping upper-boundary reflections have a similar or slightly shallower dip than linear reflections above, within the margin wedge, which might indicate that megalenses form using pre-existing planes of weakness. Movement along a pre-existing weak interface may be favoured when fluids expelled from subducting sediment reach the structure and reduce friction, which detaches a lens of margin wedge rock. Seaward, beneath the middle slope, the landward-dipping upper boundary of the megalens merges with a subhorizontal group of reflections (Fig. 3d) which might indicate a lithological boundary within the margin wedge.

Tectonic erosion has been inferred from long-term subsidence of the continental slope off Nicaragua, and the steep slope with scars of numerous landslides indicates that erosion is probably currently active[11,14]. Thus, tectonic erosion may not be limited to the region where thick crust and rough sea floor subducts, but could extend along much of the Middle America trench. However, thinning and deepening of the ocean crust, and the smaller seafloor relief towards Nicaragua, correspond to changes in tectonism along the plate boundary. Closely spaced normal faulting of the ocean plate off Nicaragua creates a 'washboard' topography. Subduction of this type of morphology has been proposed as an erosional mechanism[21]. However, the upper plate off Nicaragua is thick relative to that of northwest Nicoya; this indicates that the 'washboard' topography is either not an efficient mechanism of basal erosion or that erosion there is limited to the frontal ~10 km of the upper plate.

In addition to the erosional mechanisms discussed above, the subduction of the entire ocean pelagic-hemipelagic section indicates

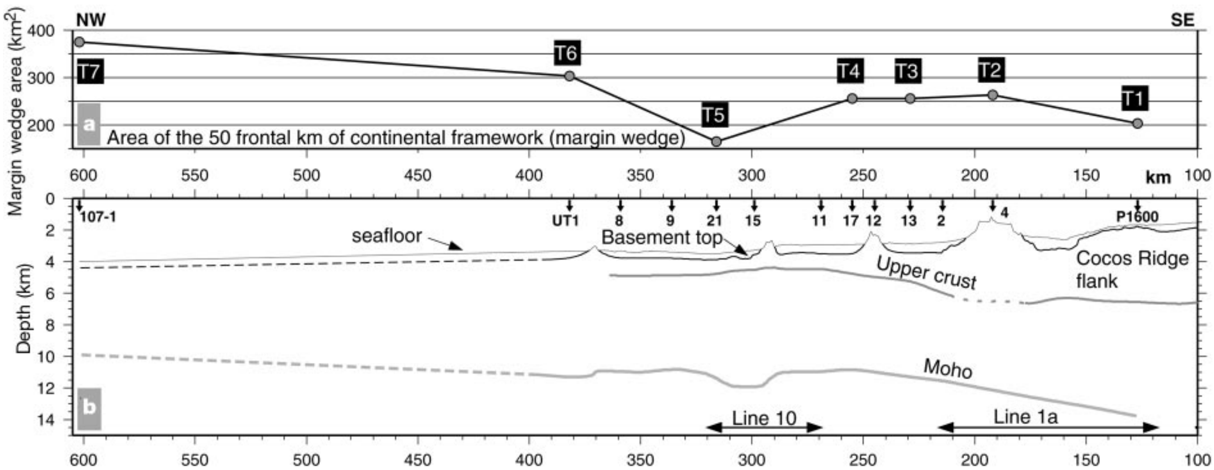

Figure 2 Comparison of continental framework thickness with the structure of the facing ocean plate. **a**, Cross-sectional area (km^2) of the continental framework (margin wedge) of the upper plate from Costa Rica to Nicaragua. Values T1–T7 are the area of the frontal 50 km of margin wedge calculated along the transects shown in Fig. 1. **b**, Crustal structure of the ocean plate along the transect in Fig. 1b. Downward-pointing arrows with numbers indicate crosspoints of transect with seismic tracks used to constrain the crustal structure. Double-headed arrows indicate extent of seismic lines along the transect. Data from refs 12, 13, 23 and this study.

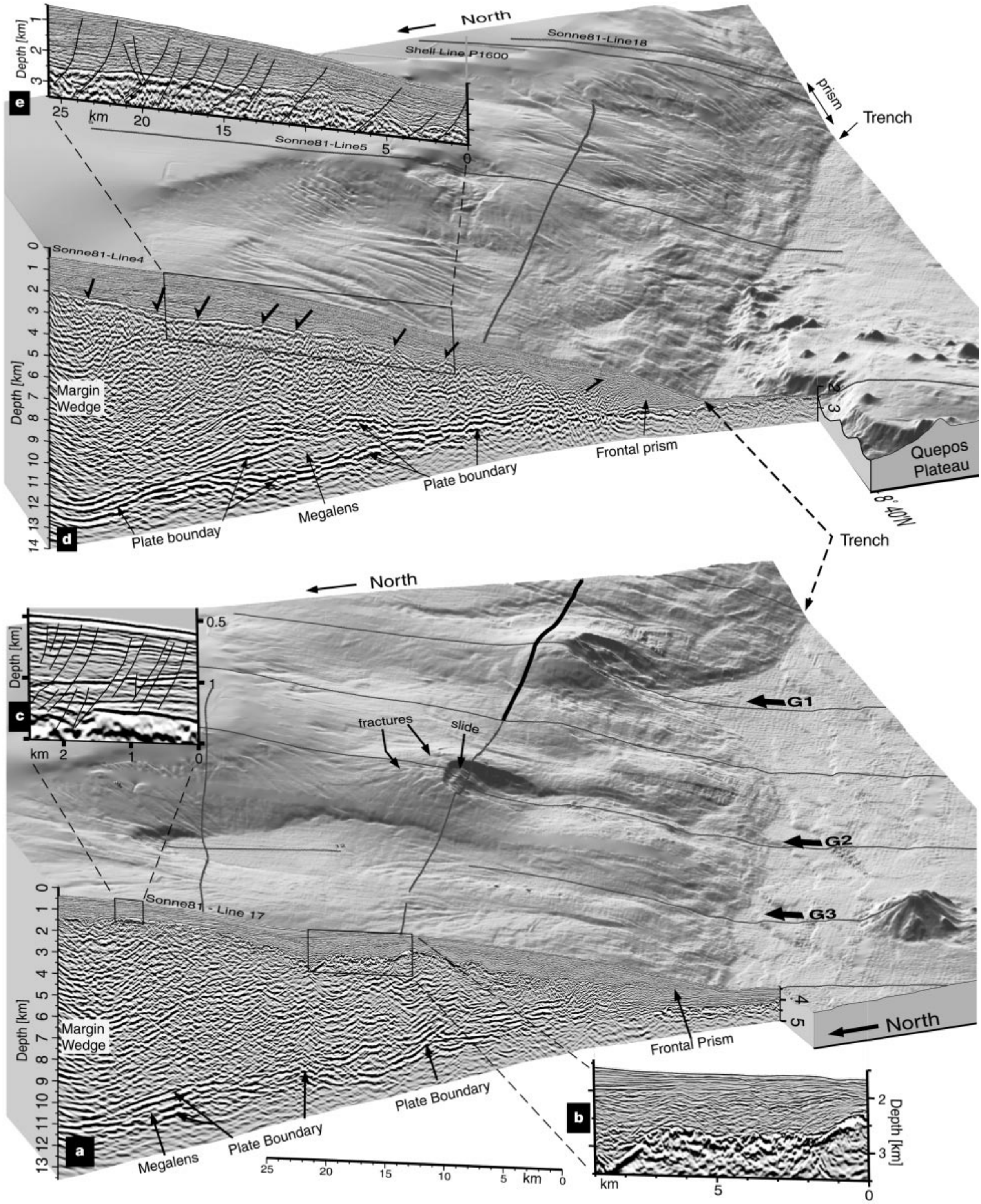

Figure 3 Prestack depth migration of Sonne-81 lines 17 and 4 projected on bathymetry perspectives. The iterative migration procedure uses velocities constrained with focusing analyses and common reflection point gathers[24]. Wide-angle data guided velocity picking at depths greater than ~5 km. Resolution at ~10 km is ~0.5 km. **a**, Line 17 is 55 km long from the toe to the upper continental slope. The line is where seamounts have recently subducted. Note the small frontal prism, the continuity of plate boundary reflections and the distinct top of the margin wedge. The frontal ~40 km of the margin have a rough margin-wedge top (inset **b**) produced by underthrusting of seamounts like those shown in the bathymetry. Arrows point to grooves in the bathymetry (G1–G3) produced by subducting seamounts, and the doming up of the sea floor indicates the location of two of those seamounts. Where the margin wedge is >6–8 km thick its top is smooth, only cut by normal faulting (inset **c**). Beneath the upper slope, plate-boundary reflections bifurcate and surround a rock megalens. **d**, Line 4 is 58 km long from the toe to the upper continental slope. The top of the margin wedge is smooth beneath the upper slope, cut by small throw normal faults (inset **e**). Fault throw grows and fault dip decreases downslope and the top of the margin wedge becomes rougher. The canyons in the upper and middle slope indicate a relatively stable environment where no seamount has recently underthrusted. Thrust faulting occurs only at the small frontal prism. The frontal prism is a distinct morphological unit, tectonically active as indicated by the disruption of the slope drainage system. Plate-boundary reflections bifurcate at ~ 6 km depth and surround a rock megalens.

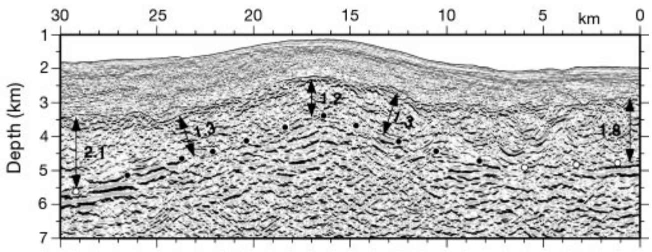

Figure 4 Active tectonic erosion by seamount tunnelling. The seismic image is a prestack depth migration of a segment of Sonne-81 line 6 over a subducting seamount. Dots mark the plate boundary, with black dots delineating the seamount flanks. This segment of the seismic line is parallel to the continental margin, and shows lateral variations in margin wedge thickness. The margin wedge is 0.5–0.7 km thinner above the subducting seamount. Extension of the upper plate by uplift above the seamount is too small to explain the thinning. Thus, thinning is probably due to tectonic erosion produced by mechanical wearing of the upper plate. The location of this cross-section is shown on Figs 1 and 3.

that hydrofracturing and piecemeal stoping[2,4,8] (an underground mining process) of the base of the upper plate by overpressured fluids may also contribute to upper-plate thinning. A body of Plio-Pleistocene sediment at the front of the margin from southern Costa Rica to Guatemala is limited to a prism less than 10 km wide[11,14,22]. Although underplating at the rear of the frontal prism might be active or an older relatively small body of accreted material may be present[19], accretion of sediment must be limited in space and time. Subduction erosion at present dominates processes off Costa Rica, and probably also extends into the Nicaraguan margin. □

Received 6 August 1999; accepted 22 February 2000.

1. Rutland, R. W. R. Andean orogeny and ocean floor spreading. *Nature* **233,** 252–255 (1971).
2. Murauchi, S. & Ludwig, W. J. Crustal structure of the Japan trench: The effect of subduction of ocean crust. *Init. Rep. DSDP* **56-57** (part 1), 463–470 (1980).
3. Scholl, D. W., von Huene, R., Vallier, T. L. & Howell, D. G. Sedimentary masses and concepts about tectonic processes at underthrust ocean margins. *Geology* **8,** 564–568 (1980).
4. von Huene, R. & Scholl D. W. Observations at convergent margins concerning sediment subduction, subduction erosion, and the growth of continental crust. *Rev. Geophys.* **29,** 279–316 (1991).
5. Lallemand, S. & Le Pichon, X. Coulomb wedge model applied to the subduction of seamounts in the Japan Trench. *Geology* **15,** 1065–1069 (1987).
6. Collot, J. Y. & Fisher, M. A. Formation of forearc basins by collision between seamounts and accretionary wedges: An example from the New Hebrides subduction zone. *Geology* **17,** 939–933 (1989).
7. Ballance, P. F. *et al*. Subduction of a large Cretaceous seamount of the Louisville ridge at the Tonga Trench: A model of normal and accelerated tectonic erosion. *Tectonics* **8,** 953–962 (1989).
8. Le Pichon, X., Henry, P. & Lallemant, S. Accretion and erosion in subduction zones: The role of fluids. *Annu. Rev. Earth Planet. Sci.* **21,** 307–331 (1993).
9. Hinz, K., von Huene, R., Ranero, C. R. & PACOMAR working group. Tectonic structure of the convergent Pacific margin offshore Costa Rica from multichannel seismic reflection data. *Tectonics* **15,** 54–66 (1996).
10. Kimura, G. *et al. Init. Rep. ODP* **170** (1997).
11. Ranero, C. R. *et al*. A cross section of the Pacific Margin of Nicaragua. *Tectonics* (in the press).
12. Stavenhagen, A. U. *et al*. Seismic wide-angle investigations in Costa Rica—a crustal velocity model from the Pacific to the caribbean Coast. *Zbl. Geol. Paläeontol.* **1,** 393–408 (1998).
13. Walther, C. H. E., Flueh, E. R., Ranero, C. R., von Huene, R. & Strauch, W. Crustal structure across the Pacific Margin of Nicaragua—evidence for ophiolitic basement and a shallow mantle sliver. *Geophys. J. Int.* (in the press).
14. von Huene, R., Ranero, C. R., Weinrebe, W. & Hinz, K. Quaternary convergent margin tectonics of Costa Rica, segmentation of the Cocos Plate, and Central American volcanism. *Tectonics* (in the press).
15. Scholz, C. H. & Small, C. The effect of seamount subduction on seismic coupling. *Geology* **25,** 487–490 (1997).
16. Wang, W. & Scholz, C. H. Wear processes during frictional sliding of rock: A theoretical and experimental study. *J. Geophys.Res.* **99,** 6789–6799 (1994).
17. Protti, M., Güendel, F. & McNally, K. in *Geologic and Tectonic Development of the Caribbean Plate Boundary in Southern Central America* (ed. Mann, P.) (Special Paper 295, Geological Society of America, Boulder, Colorado, 1995).
18. McIntosh, K., Silver, E. & Shipley, T. Evidence and mechanisms for forearc extension at the accretionary Costa Rica convergent margin. *Tectonics* **12,** 1380–1392 (1993).
19. Shipley, T. H., McIntosh, K. D., Silver, E. A. & Stoffa, P. L. Three-dimensional seismic imaging of the Costa Rica accretionary prism: Structural diversity in a small volume of the lower slope. *J. Geophys. Res.* **97,** 4439–4459 (1992).
20. Vrolijk, P. On the mechanical role of smectite in subduction zones. *Geology* **18,** 703–707 (1990).
21. Hilde, T. W. C. Sediment subduction versus accretion around the Pacific. *Tectonophysics* **99,** 381–397 (1983).
22. Aubouin, J. *et al.* Leg 84 of the deep drilling project:subduction without accretion: Middle America Trench off Guatemala. *Nature* **297,** 458–460 (1982).
23. Ye, S. *et al.* Crustal structure of the subduction zone off Costa Rica derived from OBS refraction and wide-angle reflection seismic data. *Tectonics* **15,** 1006–1021 (1996).
24. Mackay, S. & Abma, R. Depth focusing analysis using wavefront-curvature criterion. *Geophysics* **58,** 1148–1156 (1993).

Acknowledgements

We thank T. Reston for comments on the manuscript. SONNE-81 seismic reflection data were collected by the BGR.

Correspondence and requests for materials should be addressed to C.R.R. (e-mail: cranero@geomar.de).

Quantitative evidence for global amphibian population declines

Jeff. E. Houlahan*, C. Scott Findlay*†, Benedikt R. Schmidt‡, Andrea H. Meyer§ & Sergius L. Kuzmin‖

* *Ottawa-Carleton Institute of Biology, University of Ottawa, 30 Marie Curie, Ottawa, Ontario K1N 6N5, Canada*
† *Institute of Environment, University of Ottawa, 555 King Edward Street, Ottawa, Ontario K1N 6N5, Canada*
‡ *Zoologisches Institut, University of Zürich, Winterthurerstrasse 190, CH-8057 Zürich, Switzerland*
§ *Swiss Federal Statistical Office, Sektion Hochschulen und Wissenschaft, Espace de l'Europe 10, CH-2010, Neuchâtel, Switzerland*
‖ *Institute of Ecology and Evolution, Russian Academy of Sciences, Moscow 117071, Russia*

Although there is growing concern that amphibian populations are declining globally[1–3], much of the supporting evidence is either anecdotal[4,5] or derived from short-term studies at small geographical scales[6–8]. This raises questions not only about the difficulty of detecting temporal trends in populations which are notoriously variable[9,10], but also about the validity of inferring global trends from local or regional studies[11,12]. Here we use data from 936 populations to assess large-scale temporal and spatial variations in amphibian population trends. On a global scale, our results indicate relatively rapid declines from the late 1950s/early 1960s to the late 1960s, followed by a reduced rate of decline to the present. Amphibian population trends during the 1960s were negative in western Europe (including the United Kingdom) and North America, but only the latter populations showed declines from the 1970s to the late 1990s. These results suggest that while large-scale trends show considerable geographical and temporal variability, amphibian populations are in fact declining—and that this decline has been happening for several decades.

Over the past several decades, there have been reports of catastrophic declines and extirpations of amphibian species in Australia, South and Central America[13–16], and in high-altitude regions of the western United States[17]. Ancillary evidence has pointed to several possible underlying causes, including changes in local climate[18], acid precipitation[19], disease[20,21], increased UV-B irradiation[22] or various combinations thereof[23,24]. Because these reports usually document the disappearances of species from small geographical regions, extrapolations to 'global' amphibian declines are tenuous at best. To address this problem of restricted geographical coverage, we have analysed 936 amphibian population data sets collected from journal publications and technical reports, as well as unpublished data provided by herpetologists from around the world. Every effort was made to be exhaustive, and we believe